Ultrafast optics with a mode-locked erbium fiber laser in the undergraduate laboratory

Daniel Upcraft, Andrew Schaffer, Connor Fredrick, et al.

Citation: American Journal of Physics **89**, 1152 (2021); doi: 10.1119/10.0005890
View online: https://doi.org/10.1119/10.0005890
View Table of Contents: https://aapt.scitation.org/toc/ajp/89/12
Published by the American Association of Physics Teachers

INSTRUCTIONAL LABORATORIES AND DEMONSTRATIONS

The downloaded PDF for any Note in this section contains all the Notes in this section.

John Essick, *Editor*

Department of Physics, Reed College, Portland, OR 97202

Articles in this section deal with new ideas and techniques for instructional laboratory experiments, for demonstrations, and for equipment that can be used in either. Although these facets of instruction also appear in regular articles, this section is for papers that primarily focus on equipment, materials, and how they are used in instruction. Manuscripts should be submitted using the web-based system that can be accessed via the American Journal of Physics home page, ajp.aapt.org, and will be forwarded to the IL&D editor for consideration.

Ultrafast optics with a mode-locked erbium fiber laser in the undergraduate laboratory

Daniel Upcraft,[a] Andrew Schaffer,[b] Connor Fredrick,[c] Daniel Mohr,[d] Nathan Parks, Andrew Thomas, Ella Sievert, Austin Riedemann, and Chad W. Hoyt[e]
Department of Physics and Engineering, Bethel University, St. Paul, Minnesota 55112

R. Jason Jones
University of Arizona, Wyant College of Optical Sciences, Tucson, Arizona 85721

(Received 23 July 2015; accepted 5 June 2021)

We describe an ultrafast optics laboratory comprising a mode-locked erbium fiber laser, autocorrelation measurements, and a free-space parallel grating dispersion compensation apparatus. The gain spectrum of Er fiber provides a broad bandwidth capable of supporting sub-100 fs pulses centered near a wavelength of 1550 nm. The fiber laser design used here produces a train of pulses at a repetition rate of 55 MHz with pulse duration as short as 108 fs. The pulse duration is measured with a homebuilt autocorrelator using a simple Michelson interferometer that takes advantage of the two-photon nonlinear response of a common silicon photodiode. To compensate for temporal stretching of the short pulse due to group velocity dispersion in the fiber, an apparatus based on a pair of parallel gratings is used for pulse compression. A detailed part that lists in the supplementary material includes previously owned and common parts used by the telecommunications industry, which helps decrease costs of the laboratory. This provides a cost-effective way to introduce the principles of ultrafast optics to undergraduate laboratories.

https://doi.org/10.1119/10.0005890

I. INTRODUCTION

Laboratory experiences for undergraduates beyond their first year of study can provide significant opportunities for physics and engineering education and research. In an advanced laboratory, students can make hands-on contact with important historical experimental milestones and contemporary phenomena, or begin experiences with open-ended projects that approach those of a productive research laboratory. Growing attention is being given to undergraduate physics laboratory courses by researchers and educators.[1,2] New laboratories have been developed as well as formal analyses of their pedagogical aspects.[3–5] Here, we describe an ultrafast optics laboratory that is perhaps somewhat uncommon in the undergraduate setting. The concepts and required skills are used in state-of-the-art physics, engineering, and industrial settings. The fields of ultrafast optics, mode-locked fiber lasers, and frequency combs[6] are mature yet continue to find new and interdisciplinary applications.

In contrast to common ultrafast systems such as mode-locked titanium-sapphire lasers,[7] the apparatus described below is relatively inexpensive. This is in large part due to the wide availability of telecommunications components and equipment. The mode-locked fiber laser described in this manuscript can be built for approximately 7400 USD. This cost includes the purchase of a fiber fusion splicer (3470 USD). We have, however, also built a similar fiber laser that utilizes standard connectorized fiber components and does not require the fusion splicer, bringing the cost down to approximately 3900 USD. A detailed parts list for both lasers can be found in Table SI in the supplementary material.[8] The autocorrelation and dispersion compensation apparatus described below can be built for approximately 2150 USD and 1440 USD, respectively (Tables SII and SIII in the supplementary material).

The results from the apparatus described here were achieved over several semesters by undergraduate students in open-ended, course project groups as well as summer and semester research students (supplementary material Sec. S.I). Student ownership outcomes of this and other laboratories have recently been formally assessed in the context of two of Bethel University's advanced laboratory courses: Optics, and Topics in Contemporary Optics: Lasers.[9–11]

In Sec. II, we give an introduction to ultrafast optics by reviewing short-pulse descriptions in the time and frequency domains. This background is needed to understand key elements of the laser cavity design and related experiments that demonstrate the concepts of Fourier-transform-limited pulse duration, pulse chirp, pulse compression techniques, and pulse measurement techniques based on the second-order autocorrelation. A description of the ultrafast laboratory project results follows in sections briefly describing the mode-locked fiber laser (Sec. III), the autocorrelator used to measure ultrashort pulses (Sec. IV), and the parallel grating dispersion compensator used to compress pulses to their minimum duration (Sec. V and supplementary material Sec. S.V). These sections may provide guidance for an advanced laboratory instructor or undergraduate researcher in this field. They are a starting point for theoretical concepts and may clarify sometimes confusing terminology and convention. They may also provide practical reference points for building the apparatus and typical data. For example, the instructor may reasonably choose to build the apparatus in these three sections in three separate semesters of an advanced laboratory course. Alternatively, the mode-locked Er fiber laser described in Sec. III could be purchased directly from various companies[12] and used as a starting point to explore pulse propagation, amplification, and measurement (Secs. IV and V).

To support students and instructors, there is a large amount of related literature. We find Refs. 13–20 helpful for the mode-locked fiber laser, Refs. 21–23 for pulse characterization, and Refs. 18 and 23–25 for the external parallel grating dispersion compensation apparatus.

II. BACKGROUND: ULTRASHORT PULSE DESCRIPTIONS

A description of optical pulses in the time and frequency domains provides a useful example of complex Fourier transforms. Such a description is helpful in describing pulse propagation in linear and nonlinear regimes. For a more complete discussion on this background material, see Ref. 22. Neglecting spatial dependence and polarization, the electric field for a single optical pulse can be written as $E(t) = A(t)\cos(\omega_0 t + \phi(t))$, where $A(t)$ is the pulse envelope, ω_0 is the carrier frequency of the pulse, and $\phi(t)$ describes phase deviations from this average carrier frequency. A complex representation of the pulse is often convenient and can be written as $E(t) = \tilde{A}(t)\, e^{i\omega_0 t} + c.c.$, where $\tilde{A}(t) = A(t)\, e^{i\phi(t)}$ is the complex temporal envelope. The real pulse envelope $A(t)$ is often modeled as a Gaussian function for analytical convenience, and as a hyperbolic secant for a more accurate depiction of a common pulse shape (as in the case of optical solitons). Two examples for $E(t)$ are shown in Fig. 1. In this example, the chirped pulse on the left corresponds to the case where $\phi(t)$ varies quadratically along the pulse profile, resulting in a linearly varying instantaneous frequency on the pulse, $d\phi/dt \propto t$. For the unchirped pulse on the right of the figure, $d\phi/dt =$ constant.

The complex spectrum for the pulse is defined by

$$\tilde{E}(\omega) = \frac{1}{\sqrt{2\pi}}\int_{-\infty}^{\infty} E(t)e^{-i\omega t}dt = |\tilde{E}(\omega)|e^{i\Phi(\omega)}, \tag{1}$$

where $|\tilde{E}(\omega)|$ is the amplitude of the pulse spectrum, and $\Phi(\omega)$ is its spectral phase. The time and frequency domain descriptions of the pulse are equivalent, and form a Fourier transform pair, where the inverse transform of the complex spectrum gives the time-dependent electric field

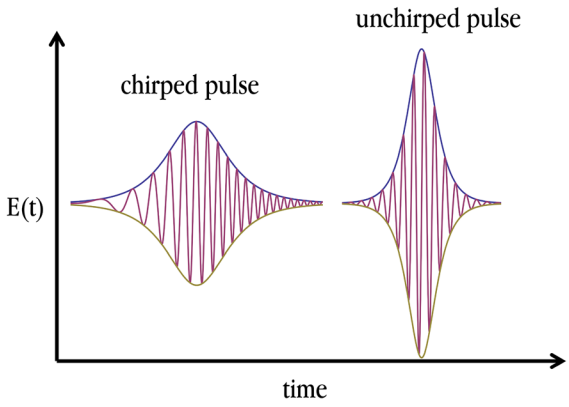

Fig. 1. Simulation of chirped (left) and unchirped (right) pulses. The pulse on the right is referred to as a Fourier-transform-limited pulse. The up-chirped pulse on the left results from propagation through a material with normal dispersion (positive GDD, or $\beta'' > 0$ [see the supplementary material Sec. S.II]) since the lower frequencies arrive at an earlier time.

$$E(t) = \frac{1}{\sqrt{2\pi}}\int_{-\infty}^{\infty} \tilde{E}(\omega)e^{i\omega t}d\omega. \tag{2}$$

This Fourier relationship between time and frequency is a good opportunity to connect the use of complex Fourier transforms to other examples with which advanced students may be more familiar. These include the spatial analog for light propagation, where the near and far fields are related by a Fourier transform, and the Heisenberg uncertainty relations of quantum mechanics. The inverse relationship between the pulse duration, τ_p, and the corresponding spectral bandwidth, $\Delta\nu$, can then be seen as a direct result of the properties of the Fourier transform: $\tau_p \cdot \Delta\nu \gtrsim \frac{1}{2}$. The exact relations for various pulse shapes are given in supplementary material Sec. S.II.

Propagation can alter pulses of light either linearly or nonlinearly, depending upon the material through which the pulses propagate, such as in the example shown in Fig. 1. In the case of linear pulse propagation, the complex spectrum of a pulse will be multiplied by a frequency-dependent spectral phase term. This spectral phase is affected by dispersion or the phenomenon where the phase velocity of light depends on its frequency. Fundamental parameters to describe the effect of dispersion on pulse propagation include the well-known propagation constant $k(\omega) = \frac{\omega}{c}n(\omega)$, where $n(\omega)$ is the frequency-dependent index of refraction and c is the speed of light in vacuum. The second derivative of this term with respect to angular frequency ω is called group velocity dispersion (GVD) and is represented by k''. Related to this is the group delay dispersion (GDD), which is defined as $k''z$, where z is the propagation distance through the material. The propagation constant is also often written as $\beta(\omega)$ when dealing with the effective refractive index of optical fiber. Dispersion can cause chirp where the frequency of the light increases (positive- or up-chirp) or decreases (negative- or down-chirp) with time and propagation. These concepts of linear and nonlinear propagation of pulses are developed comprehensively in supplementary material Secs. S.II and S.III, respectively.

III. MODE-LOCKED LASER

The mode-locked fiber laser is an advanced laboratory experiment that alone could take a full academic semester to complete. In this section, we describe the basic components needed to construct the oscillator and obtain lasing, as well as specific components needed to generate ultrashort pulses. Components are readily available thanks to the telecommunications industry, which relies heavily on erbium fiber technology. There are several different mode-locking mechanisms that can be used to force the laser into a state that favors short pulses over continuous-wave (cw) oscillation. Here, we choose nonlinear polarization rotation,[13] described in more detail later. This common mode-locking technique often produces the lowest noise and shortest pulse durations directly from an erbium fiber laser cavity. Alternative mechanisms that may simplify the design include fast saturable absorbers, which are available commercially.[26–28]

A diagram of the erbium-doped fiber laser is shown in Fig. 2. The design is based on the stretched-pulse mode-locked laser of Ref. 13. Except for the short, free-space section (red line), the solid lines indicate single-mode optical fiber, which confines light to the small fiber core ($\sim 6\,\mu$m) that is surrounded by a 125-μm-diameter cladding. Fiber is sold with a protective coating (and sometimes a thicker, colored jacket), which must be removed in order to directly splice different fibers and fiber-based components together. The x symbols in Fig. 2 indicate approximate locations of splices between different sections of the oscillator. Splicing the fibers directly together requires the use of a fusion splicer. Alternatively, connections between different fibers and fiber-based components can be made using standard threaded connectors, which place two fiber ends in physical contact with each other. The use of mechanical connections is often more convenient, but comes at the price of increased losses and back reflections. The lowest loss connector is an angled-face connector known as FC/APC. Losses from mechanical connections can be minimized by using an index matching fluid between fiber tips. The parts for a complete connector-based laser are described in Table SI.

Several components in the oscillator are standard telecommunications devices. The wavelength-division multiplexer (WDM) combines light from the 974-nm pump laser with the 1550-nm signal light into a single core of optical fiber that can then be connected to the gain fiber. The graded index (GRIN) lenses in Fig. 2 are integrated into the fiber and provide collimation into free space and coupling back into the fiber. The optical isolator in the cavity forces oscillation in one direction. The isolator outside the cavity minimizes feedback to the cavity from optical back reflections downstream, which can destabilize the mode-locking process. The free-space section of the cavity is needed solely for the purpose of mode-locking the laser (to be described shortly) and could be replaced with an appropriate saturable absorber. The free-space section includes half and quarter waveplates, which enable control over the complex polarization state of the light, as well as a polarizing beam splitter (PBS), which passes one linear polarization and rejects the orthogonal polarization.

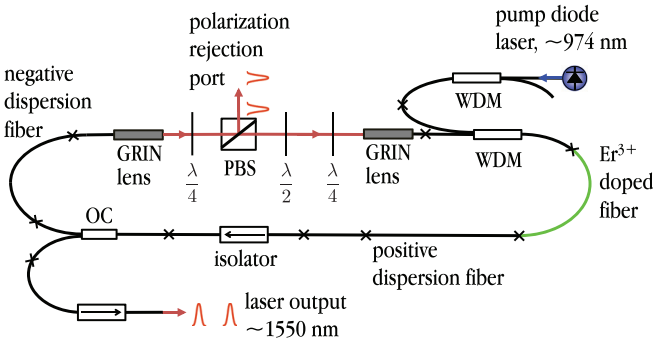

Fig. 2. Er^{3+}-doped nonlinear polarization mode-locked fiber laser. Approximate splice locations are indicated with an x symbol. WDM: wavelength division multiplexer that combines different wavelengths; OC: output coupler; PBS: polarizing beam splitter; GRIN: graded index lens collimator; $\lambda/2(4)$: half- (quarter-)wave plate.

The laser gain is provided by erbium-doped single-mode fiber ($\sim$20 dB gain[29]) shown as the green portion of the cavity in Fig. 2. This relatively high gain leads to the possibility of high output coupling (the OC component in the figure), as much as 50%. In order to achieve laser oscillation, the cavity's gain must be greater than the losses, which means minimizing losses at fiber connections and careful alignment of the free-space portion. Making connections with a fusion splicer typically results in lower losses than coupling with mechanical connectors. Typical threshold pump laser currents—the point at which the gain just equals the losses—for the laser in Fig. 2 are 55 mA for spliced connections and 115 mA for mechanical connectors. Since the threshold pump current corresponds to cavity loss, it is helpful to minimize this value when making new connections, adding components, or optimizing the free-space portion of the cavity.

When pumped, the gain section glows green even though the lasing wavelength is centered near 1550 nm and the pump wavelength is at 974 nm. This can be explained by the erbium atomic excitation process. As shown in Fig. 2, pump light is coupled into the cavity using a WDM and excites the erbium atoms via the ${}^4I_{15/2} \rightarrow {}^4I_{11/2}$ energy state manifold transitions (see Fig. 3). The laser transition takes place between the broad ${}^4I_{13/2}$ and ${}^4I_{15/2}$ manifolds leading to a gain bandwidth of over 50 nm. The gain pumping process includes the possibility of excited state absorption from the ${}^4I_{11/2}$ manifold to the higher energy state manifolds with the pump laser at 974 nm.[30] Subsequent decay pathways to the ground state can produce green fluorescence. This is a way to monitor lasing. When the cavity changes from not lasing to lasing (e.g., during alignment of the free-space cavity section), for the same pump laser power, the green glow will dim due to the laser mode's use of the gain via stimulated emission.

When first aligned for lasing, the oscillator in Fig. 2 will likely operate in a cw output state. Typical cw output powers are in the range of 1–5 mW. To force the laser into a state that favors generation of a single intracavity short pulse, several common methods of passive mode-locking are possible, including saturable dyes, carbon nanotube solutions applied to fiber tapers[15] or between connectors,[27] and saturable semiconductor structures made from quantum wells or quantum dots.[31] The free-space section of the cavity shown in Fig. 2 may be replaced with such saturable absorbers to obtain mode-locking.

Here, the mechanism for mode-locking is provided by a nonlinear rotation of light polarization[16] during propagation in the cavity's single-mode fiber. This rotation arises due to variation in intensity between orthogonal polarization directions in the fiber, resulting in different phase shifts between polarization components (due to the silica fiber's nonlinear

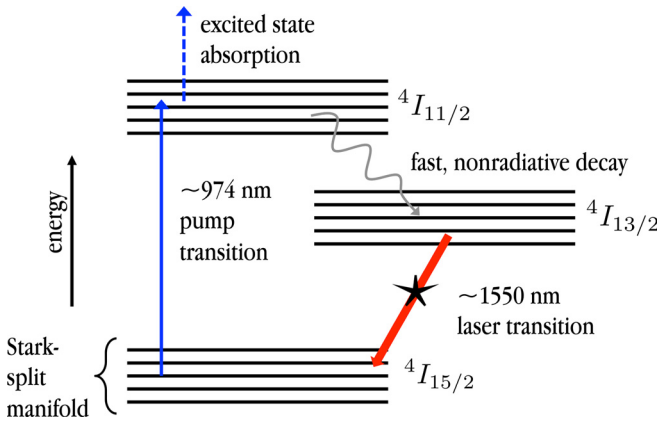

Fig. 3. Er^{3+}-doped silica fiber energy level structure (not to scale). Transitions are inhomogeneously broadened due to local Stark-shifting electric fields. Pumping for the $^4I_{13/2} \rightarrow {}^4I_{15/2}$ laser transition can also be done at 1480 nm directly to the top of the $^4I_{13/2}$ manifold. Excited state absorption of the pump light from the $^4I_{11/2}$ manifold leads to green fluorescence.

index of refraction, n_2). This results in a polarization rotation, a behavior that is like an intensity-dependent optical wave plate. When the polarization control elements (waveplates) in the free-space section of the cavity are properly adjusted, a short pulse will propagate around the cavity and see minimal loss when passing through the polarization beam splitter (PBS). However, for the lower peak intensity of cw light, which does not undergo nonlinear polarization rotation, the losses at the PBS will be high. A short pulse will therefore see more net round trip gain than that of the background cw light, forcing the laser to evolve to support only a single short pulse.

The laser in Fig. 2 is mode-locked by adjusting the quarter- and half-wave plates in the free-space section of the cavity and monitoring the output power and pulse repetition rate or pulse spectrum. When mode-locked, repeated peaks will be seen on a fast photodiode at the output and the pulse spectrum will dramatically change from a narrow peak to a broad spectrum (>10 nm). Mode-locking is often found for waveplate orientations where the cw power is very low (high loss for cw light) and switches suddenly to a higher power condition with short pulse operation (low loss state). We note that aligning the waveplates for mode-locking can take some effort, searching in a random-walk fashion over a large parameter space. It can be helpful to only move one waveplate at a time so as to not miss a potential mode-locking orientation. When one waveplate is rotated fully, one of the others can be adjusted slightly and the first can be rotated fully again. This process can be extended to the third waveplate if the orientations of the second are exhausted as well. If the single-mode fiber that makes up most of the laser cavity is not fastened to the table (e.g., taped down), repositioning of the fiber can change the optimum position of the waveplates due to stress-induced birefringence. Since the lifetime of the upper laser state is significantly longer than a typical cavity round-trip time, mode-locked average output powers are similar to optimized cw powers (typically 1–5 mW).

The lengths of different fibers in the laser cavity shown in Fig. 2 are listed in Table I. As discussed above, generating and maintaining the shortest pulses requires careful attention to the net round-trip dispersion. In fact, the laser may not mode-lock at all if there is not proper dispersion. The shortest pulses come from a laser oscillator that has a balance between opposite signs of β''. Stable, soliton mode-locking can be achieved in the laser oscillator shown in Fig. 2 by assembling a cavity with net negative (anomalous) dispersion (e.g., SMF-28) in the cavity. Soliton mode-locking can often be identified by a characteristically multi-peaked spectrum. These peaks are phase-matched sidebands originating from the excess energy the soliton sheds in order to maintain its constant energy and shape.[32] Related to this is the fact that soliton pulses in such a fiber laser are constrained in duration and energy. In other words, they may not take full advantage of the large erbium gain bandwidth or broadening nonlinearities in the cavity.

The dispersion-balanced, stretched-pulse fiber laser of Fig. 2 avoids the constraints of soliton pulse operation.[13] Alternate sections of positive and negative dispersion single-mode fiber allow the pulse to temporally expand and contract in a single cavity round-trip. High energy pulses drive large nonlinear broadening at cavity locations where pulse width is minimal, while zero or slightly positive net dispersion in the cavity avoids soliton solutions.[14] This leads to spectrally broad pulses, potentially broader than the gain bandwidth due to strong nonlinearities, that are sometimes highly chirped. However, extra-cavity dispersion compensation, either through proper choice of fiber or using gratings as demonstrated in Sec. V, can compress pulses to the sub-100 fs level.[13]

Components such as WDMs typically use single-mode fiber with negative (anomalous) dispersion at 1550 nm. The cavity in Fig. 2 uses the Er^{3+}-doped gain fiber and fibers with trade names DCF3 and DCF38 for positive (normal) dispersion to balance the negative cavity dispersion. Propagation loss at splices can be minimized by matching fiber core radii (or the laser mode size). For example, in Fig. 2 we spliced the following fiber sequence: Er gain fiber, DCF38, DCF3, and SMF-28. These fibers have the following respective sequence of laser mode sizes in μm: 6.5, 6.01, 8.1, and 10.4. For this cavity, a 20% output coupler is near optimum, yielding ~5.5 mW average power. The free space section is approximately 12 cm. The WDM between the 300 mW pump laser diode and the WDM that couples pump light into the cavity isolates the pump laser diode from the spectrally broad amplified spontaneous emission from the gain section.

IV. PULSE CHARACTERIZATION

The pulse repetition rate from the mode-locked laser in Fig. 2 can be measured directly with a fast photodiode. This is also a helpful way to monitor the onset of mode-locking.

Table I. Net single-mode fiber cavity dispersion computation example.

Fiber	Length (cm)	β'' [ps^2/km]
SMF-28	89	−23[a]
Corning Flexcor 1060	56	−7[a]
DCF38, Corning Vascade S1000	56	47[b]
DCF3, Corning Vascade LS+	19	3.8[b]
Er^{3+}-doped	71	6.1[c]
Net cavity dispersion	···	0.007 **ps^2**

[a]References 13 and 14, consistent with modeling.
[b]Thorlabs specifications.
[c]Modeling estimate.

Figure 4 shows the signal from an InGaAs photodetector (Thorlabs DET01CFC, specified 1.2 GHz bandwidth, and <1 ns rise time). This detector is not fast enough to fully characterize the 100-fs pulses, but it can measure the repetition rate. The data in Fig. 4 show a pulse period of 18 ns, which corresponds to a repetition rate of ∼55 MHz and a cavity length of ∼3.7 m using a nominal fiber index of refraction of $n = 1.5$.

Sub-picosecond light pulses from a mode-locked laser can be measured using the intensity correlation between the pulse and a time delayed version of itself using an interferometer as shown in Fig. 5.[33] We consider a pulse with field $E(t)$ that is coincident on a linear photodetector with a time-delayed version of itself, $E(t-\tau)$. The resulting photocurrent is proportional to the time average of the optical power, which is proportional to $E(t)E^*(t-\tau)$. Using the convolution theorem, one can show that the measured signal, as a function of the delay τ, corresponds to the Fourier transform of the pulse's power spectrum, $|\tilde{E}(\omega)|^2$. Any spectral phase information is therefore lost. As a result, a chirped pulse will show the same signal as a Fourier-transform-limited pulse with the same spectrum.

A second-order autocorrelation, however, will yield information about the pulse duration. (Special techniques such as frequency-resolved optical gating[34] are generally necessary to completely characterize the pulse, however, including any pulse asymmetry since autocorrelations are inherently symmetric regardless of pulse shape.) This can be obtained by using a detection system with a nonlinear, second-order response (e.g., second-harmonic generation). In this case, the resulting signal is proportional to

$$S(\tau) = \int_{-\infty}^{\infty} < |(E(t) + E(t-\tau))^2|^2 > dt, \tag{3}$$

where the angled brackets indicate a time average over the high-frequency carrier oscillations and the integral indicates integration over the pulse envelope. Following the treatment of Ref. 22, the signal can be written as

$$S(\tau) = X(\tau) + \mathrm{Re}\left[4Y(\tau)e^{i\omega_0\tau}\right] + \mathrm{Re}\left[2Z(\tau)e^{i2\omega_0\tau}\right], \tag{4}$$

where Re indicates the real part. The lettered terms $X(\tau)$, $Y(\tau)$, and $Z(\tau)$ on the righthand side in Eq. (4) are time

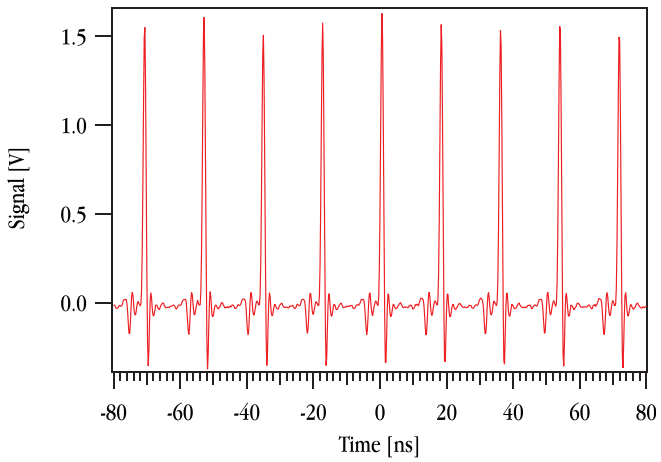

Fig. 4. Pulses from the mode-locked laser oscillator obtained with an InGaAs photodetector with a specified 1.2 GHz bandwidth and <1 ns rise time.

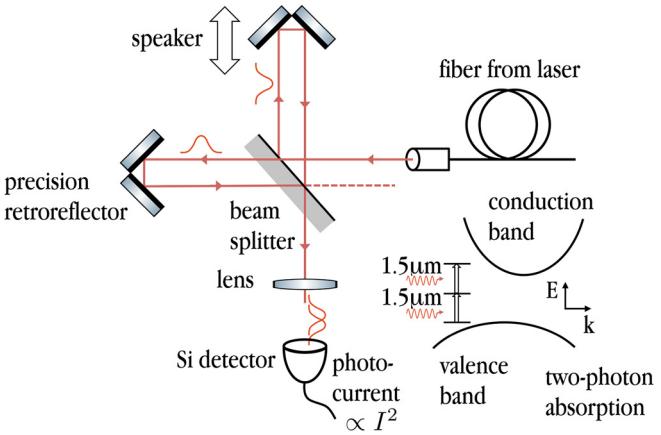

Fig. 5. Autocorrelator (AC). The second-order correlation between the laser pulse and a delayed version of itself is enabled by two-photon absorption in a simple silicon detector as shown in the indirect bandgap diagram at lower right, where the photocurrent is proportional to the square of intensity. The detector has a 1 MHz bandwidth; the speaker frequency can be used to include (interferometric AC) or average over (intensity AC) the interference fringes.

averages of the products of fields from each arm (order of E^4). They are separated in Eq. (4) according to harmonics of $\omega_0\tau$.

The first term, $X(\tau)$, is proportional to the intensity autocorrelation. The second and third terms in Eq. (4) contain interference terms, which can be used to extract phase information about the pulse. The variation in the terms containing $Y(\tau)$ and $Z(\tau)$ leads to interference fringes in the autocorrelation during measurement with a photodetected frequency related to the driving amplitude and frequency of the speaker used to scan the delay, $f_{fringe} = \frac{4d}{\lambda} \cdot f_{delay}$, where d is the amplitude, λ is the center wavelength, and f_{delay} is the driving frequency. For example, if the speaker is moved through 100 photodetected fringes in half its period of 50 ms, $d = 100\frac{\lambda}{2}$ and the photodetected fringes have a frequency of approximately 4 kHz. Therefore, when the driving frequency is sufficiently high compared to the photodetection bandwidth scaled by $\sim\frac{\lambda}{d}$, the rapidly varying terms containing $Y(\tau)$ and $Z(\tau)$ can be washed out, leaving only the intensity autocorrelation signal $X(\tau)$. All three autocorrelation terms are explicitly given in supplementary material Sec. S.IV.

The scanning Michelson interferometer used for the autocorrelation is shown in Fig. 5 and a photograph in Fig. 6. The beam is split into two arms and displaced on its return via precision hollow gold retroreflectors. These mirrors minimize feedback to the laser and aid in alignment. One retroreflector is mounted in the center of a common loudspeaker and driven at low amplitude and frequency (≲20 Hz). The retroreflector is attached to the center of the loudspeaker with epoxy. The retroreflector in the other arm is mounted on a precision linear stage, which is necessary to find the zero-delay position (where the optical path length is the same in both arms). We have also built a similar apparatus with planar mirrors instead of the more expensive retroreflectors. This choice of optics works well, although slight misalignment may be necessary to avoid feedback to the laser. To obtain only the intensity autocorrelation, the speaker is driven at higher frequency/amplitude such that the interference fringes are washed out (∼20 Hz). For the full interferometric autocorrelation, the speaker is driven at low frequencies (<1 Hz) with a detector bandwidth of 1 MHz.

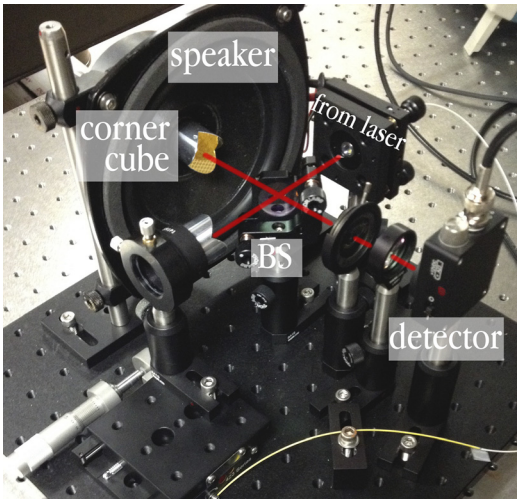

Fig. 6. Autocorrelation apparatus. The hole spacing on the breadboard and table is one inch. The precision hollow gold corner cube is mounted on an inexpensive loudspeaker to interfere a pulse with itself with variable delay on the silicon photodiode. Preceding the detector are an iris and lens ($f \approx 2.5$ cm). BS: beam splitter.

In either case, care should be taken to avoid attenuating the signal due to detection bandwidth.

The nonlinear detection is obtained using the two-photon photocurrent from a common silicon photodiode. For silicon, $E_{bg}/2 < E_{photon} < E_{bg}$, where E_{bg} is the indirect band gap energy of silicon and E_{photon} is the photon energy of the 1550-nm light pulse.[35,36] We verified the second-order response ($S \propto I^2$) of the photodetector by measuring the signal as a function of average power at the detector. These data are shown in the inset of Fig. 7 and show a quadratic dependence—consistent with two-photon absorption—up to 13 mW. Note that a two-photon signal is only seen when mode-locked.

Figure 7 shows the measured interferometric autocorrelation for the mode-locked Er fiber laser in Fig. 2. One advantage of the interferometric autocorrelation is that the interference fringes between the two arms of the interferometer can be used to calibrate the time axis: the measured phase of the interferometric signal is $\omega_0\tau$. More specifically,

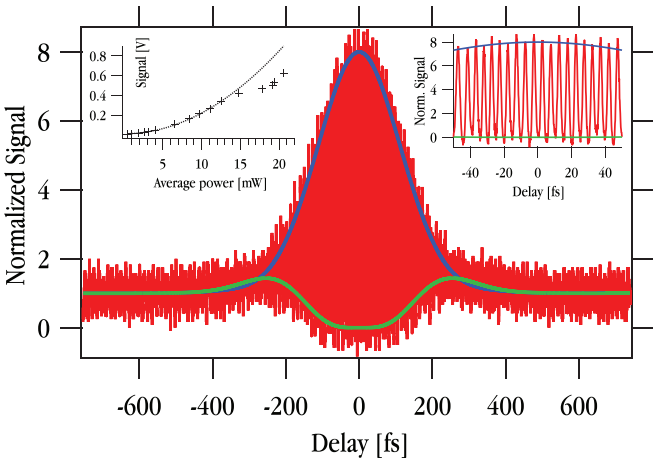

Fig. 7. Interferometric autocorrelation trace. The right inset plots the fringes around zero delay that correspond to the center optical frequency of the pulse spectrum. The left inset shows the two-photon response ($\propto I^2$) of the common silicon photodetector to pulses at 1550 nm.

the time axis can be calibrated by multiplying it by the ratio of the period of the light (c/λ where the central wavelength $\lambda = 1550$ nm) to the period of the measured autocorrelation interference fringe.

To confirm that the measured signal is accurate, one can check the signal to background ratio when aligning. From Eq. (3), we can see that for long delays, when the pulses from each arm no longer overlap, a signal background proportional to $E(t)^4 + E(t-\tau)^4 = 2E^4$ should be measured. At zero delay ($\tau = 0$), a signal proportional to $|E(t) + E(t)|^4 = 16E^4$ should be measured. Therefore, the interferometric autocorrelation should have a signal to background ratio of 8:1. Similarly, using only the intensity autocorrelation term $X(\tau)$ from Eq. (4), the intensity autocorrelation will yield a ratio of 3:1. This is outlined in supplementary material Sec. S.IV, where $X(\tau)$ is expanded.

Significant chirp on a pulse due to dispersion in propagation results in a distinctive distortion of the interferometric autocorrelation, with a reduction in the fringe contrast. An example of an interferometric autocorrelation with significant pulse chirp is shown in Fig. 9(a). Here, the output pulse from the laser was passed through a fiber amplifier, where the combination of dispersion and self-phase modulation added significant chirp.

Linear pulse chirp (quadratic phase modulation) can be easily modeled and compared to autocorrelation data by assuming a symmetric, Gaussian pulse envelope of the form: $E_g(t) = \exp\left[-(1+ia)(t/\tau_{p,g})^2 - i\omega_0 t\right] + c.c.$, where $\tau_{p,g}$ is the FWHM of the pulse duration, and a is a dimensionless parameter that determines the amount of chirp on the pulse.[22] For nonzero a, this pulse has an instantaneous frequency, $d\phi(t)/dt$, that is linearly dependent on time (see pulse on left in Fig. 1). The autocorrelation signal [Eq. (3)] for $E_g(t)$ can be determined analytically. We used the envelope of the resulting analytical solution to analyze the autocorrelation in Fig. 7. The upper and lower envelopes of the analytic expression are fit to the data using a and $\tau_{p,g}$ as parameters. From this fitting procedure, we estimate $\tau_{p,g} \approx 220$ fs and $a \approx 2$.

The spectrum of the Er fiber laser was measured using an optical spectrum analyzer and is shown in Fig. 8. As discussed previously, the inverse Fourier transform of this spectrum gives the minimum possible pulse duration. If one assumes a common pulse shape such as a Gaussian or hyperbolic secant (see the supplementary material Sec. S.II), the relationship between pulse duration τ_p (FWHM), and the spectral width, $\Delta\nu$ (FWHM), is already known. This can be used to make an estimate of the minimum pulse duration. For example, in Fig. 8 the width of the pulse spectrum, 27.8 nm, corresponds to a bandwidth-limited pulse duration of $\tau_p = 159$ fs, assuming a Gaussian pulse envelope. The autocorrelation measurement in Fig. 7 shows a 38% increase in the minimum possible pulse duration. This is not uncommon, as propagation of the pulse through various amounts of fiber can quickly add chirp to the pulse. A qualitative measure of chirp in an interferometric autocorrelation can be obtained from the size of the upward indents in the bottom of the signal, such as those seen at about a ± 200 fs delay in Fig. 7. The larger these indents are, the more chirp the pulse contains.

V. PARALLEL GRATING DISPERSION COMPENSATOR

Pulses often emerge from the mode-locked laser with some degree of chirp. Even nearly chirp-free soliton pulses

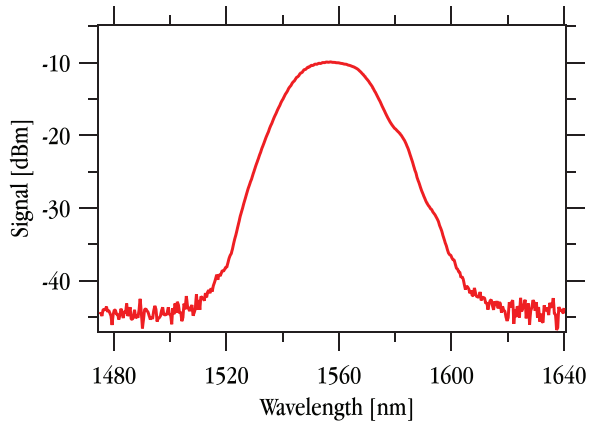

Fig. 8. Pulse spectrum from mode-locked laser oscillator output. The full width at half-maximum (FWHM) is 27.8 nm, which corresponds to a bandwidth-limited pulse duration of 159 fs, assuming a Gaussian pulse envelope. The FWHM can be determined with a linear scale or by measuring the width −3 dBm from the maximum in a logarithmic scale such as the one shown here.

experience dispersion in extra-cavity fiber. Several methods of removing chirp are used in practice, including adding fibers with appropriate lengths and signs of β''. Here, we demonstrate temporal compression by using a pair of high-efficiency transmission gratings to spatially distribute the pulse spectrum to control relative path lengths and therefore relative delay (GDD) across the pulse spectrum. A more complete description of the apparatus and concepts can be found in the supplementary material Sec. S.V.

We tested the effect of the grating dispersion compensator (compressor) by measuring the pulses from the stretched-pulse laser in Fig. 2 before and after compression. We first amplified the pulses after the oscillator to increase the measurement signal-to-noise ratio. The amplifier comprised a 280 mW laser diode at 974 nm that pumped a 58 cm Er^{3+}-doped gain fiber, copropagating with the light from the oscillator. WDMs after the gain section filter the residual pump light. Interferometric autocorrelation traces are shown for pulses following the amplifier and parallel grating dispersion compensator in Figs. 9(a) and 9(b), respectively. (Note the different horizontal scales.) The amplifier can broaden the spectrum through the nonlinear process of self-phase modulation as seen in the inset of Fig. 9(b). The average laser power into the autocorrelator directly after the amplifier was 21 mW. The average power was 17 mW just before coupling into the fiber to the autocorrelator after the dispersion compensator (see Fig. S1 in supplementary material Sec. S.V). With careful grating alignment, spatial mode quality can be sufficient to couple greater than 80% back into a single-mode fiber.

The grating compressor removed much of the chirp and shortened the pulse. We optimized the grating separation by monitoring the autocorrelation. The positive dispersion introduced by the fiber amplifier (4 m, 0.19 ps^2 net dispersion) created a strongly up-chirped pulse as shown in Fig. 9(a). The grating compressor introduces a net negative GDD, allowing us to minimize the overall second order dispersion by adjusting the grating separation. We found an optimal grating separation of 3.5 mm, which corresponds to $\beta'' \cdot l = -0.086$ ps^2 according to Eq. (S10) with a grating line density of 966 l/mm.

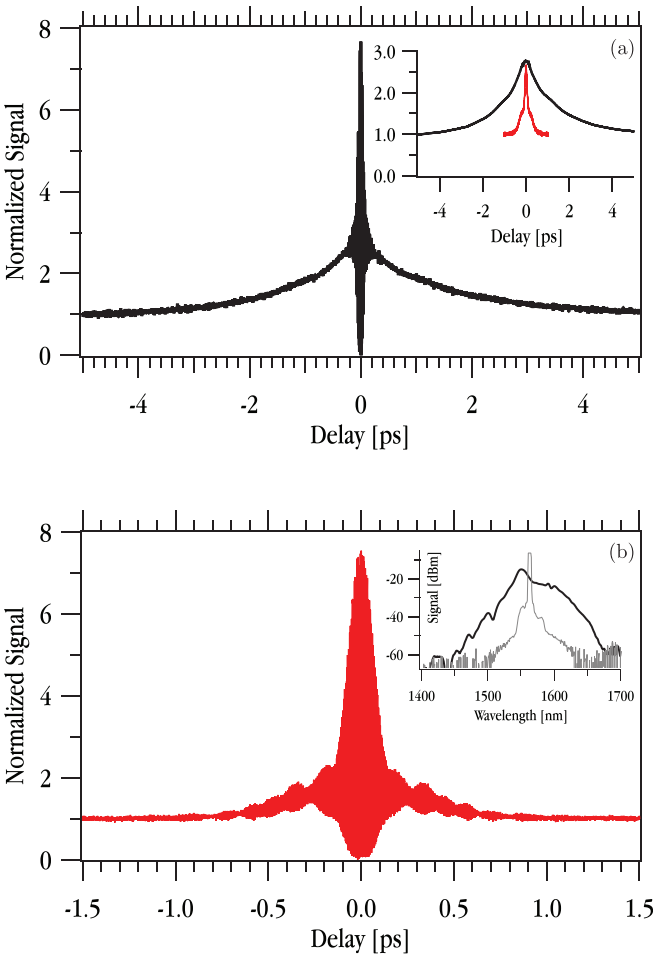

Fig. 9. Autocorrelations (ACs) of pulses after the pre-amplifier (a, black) and after the grating dispersion compensator (b, red). The corresponding intensity ACs are shown in the inset of (a). The pulse spectrum after the amplifier (black) and the cw oscillator spectrum (gray) are shown in the inset of (b). Note that the horizontal scales of (a) and (b) are different.

Assuming a Gaussian pulse envelope, a fit to the narrow portion of the intensity autocorrelation in the inset of Fig. 9(a) yields a pulse width of 108 fs, FWHM, a reduction in chirped pulse width by a factor of thirteen. Fifty percent of the area underneath the autocorrelation data is contained in this Gaussian fit. The intensity autocorrelation in the inset of Fig. 9(a) was obtained by averaging the interferometric autocorrelation. A software time-averaging procedure is equivalent to increasing the frequency of the speaker in Fig. 5. For example, the intensity autocorrelation in the inset of Fig. 9(a) was obtained by increasing the speaker frequency from 5 mHz (interferometric) to 1 Hz for the same amplitude. The pedestal on the autocorrelation is likely due to higher-order chirp (e.g., quadratic, β'''). The pulse spectrum after the amplifier is shown as the black trace in the inset of Fig. 9(b). For comparison, the continuous-wave oscillator spectrum is shown as the gray trace in the inset of Fig. 9(b).

VI. FURTHER WORK

We have described results and experimental details of an undergraduate ultrafast optics advanced laboratory using relatively low-cost components. The stretched-pulse mode locked Er^{3+} fiber laser can be built for ∼7400 USD (see the

detailed parts list in Table SI in the supplementary material). Instead of connecting fibers with a user-friendly fusion splicer, the cost of which is roughly half the total, one may instead use FC/APC connectors at fiber junctions. We have recently built such a laser that produces pulses of 108-fs duration at a cost of 3900 USD. The mode-locking mechanism could be simplified by using a fast saturable absorber such as a carbon nanotube (CNT) solution.[37,38]

The spectral data shown here were obtained with a relatively expensive optical spectrum analyzer (OSA, Ando AQ6315B). Many salient features of ultrashort pulses (autocorrelation analyses, dispersion management, repetition rate) can be observed without an OSA. Instead, a relatively affordable near-infrared spectrometer could be built using a linear InGaAs array and a grating, which could be calibrated using the first and second order of the 974-nm pump diode. An even less expensive option might use concave mirrors and a NIR-blazed grating mounted on a small stepper motor. In this constant deviation imaging monochromator, the motion is carefully calibrated and controlled to scan spectra across a small InGaAs photodiode.

A single mode-locked laser such as the one described here can provide a link between optical and radio frequency sources or be used for spectroscopy purposes if extended into an optical frequency comb.[39] Designs for such fiber frequency combs have become common and well-documented[28] and could provide a foundation for future advanced laboratories.

ACKNOWLEDGMENTS

Funding for this undergraduate advanced laboratory project is provided by the National Science Foundation EIR No. 1208930. The authors appreciate assistance from Tsung-Han Wu.

[a]Current address: University of Minnesota, Minneapolis, Minnesota.
[b]Current address: Honeywell, Golden Valley, Minnesota.
[c]Current address: University of Colorado, Boulder, Colorado.
[d]Current address: Seagate, Bloomington, Minnesota.
[e]Electronic mail: hoycha@bethel.edu; Current address: Honeywell, Plymouth, Minnesota.

[1]Recent advanced laboratory conferences include (1) Lab Focus 1993, Boise State University, Boise, ID (1993) sponsored by the NSF through the American Association of Physics Teachers (AAPT) (2) 2012 Conference on Laboratory Instruction Beyond the First Year of College, University of PA and Drexel University, Philadelphia, PA (2012) sponsored in part by the NSF, AAPT, APS (3) 2015 Conference on Laboratory Instruction Beyond the First Year, University of Maryland, College Park, MD, sponsored the NSF, AAPT.
[2]See <www.aapt.org/Resources> for "AAPT Recommendations for the Undergraduate Physics Laboratory Curriculum" (last accessed November, 2014).
[3]Benjamin M. Zwickl, Noah Finkelstein, and H. J. Lewandowski, "The process of transforming an advanced lab course: Goals, curriculum, and assessments," Am. J. Phys. **81**, 63–70 (2013).
[4]Anna Karelina and Eugenia Etkina, "Acting like a physicist: Student approach study to experimental design," Phys. Rev. Spec. Top. **3**, 020106 (2007).
[5]N. Holmes and D. Bonn, "Doing science or doing a lab? Engaging students with scientific reasoning during physics lab experiments," in *Proceedings of the Physics Education Research Conference* (AIP Press, College Park, MD, 2013).
[6]Scott A. Diddams, "The evolving optical frequency comb [invited]," J. Opt. Soc. Am. B **27**, B51–B62 (2010).
[7]T. D. Donnelly and Carl Grossman, "Ultrafast phenomena: A laboratory experiment for undergraduates," Am. J. Phys. **66**, 677–685 (1998).
[8]See supplementary material at https://www.scitation.org/doi/suppl/10.1119/10.0005890 for additional background material on linear and nonlinear propagation of pulses, autocorrelation, and the parallel grating dispersion compensator as well as parts lists to build the apparatus described in this work.
[9]J. Stanley, D. R. Dounas-Frazer, L. Kiepura, and H. J. Lewandowski, "Students' ownership of projects in the upper-division physics instructional laboratory setting," in *Physics Education Research Conference 2015*, College Park, MD, 29-30 July 2015 (AIP Press, College Park, MD, 2015): available at https://www.compadre.org/per/perc/2015/Detail.cfm?id=6336.
[10]J. Stanley, "Investigating student ownership of projects in upper-division physics laboratory courses," in *Proceedings of the American Physical Society March Meeting* (American Physical Society, Baltimore, MD, 2016).
[11]Dimitri R. Dounas-Frazer, Jacob T. Stanley, and H. J. Lewandowski, "Student ownership of projects in an upper-division optics laboratory course: A multiple case study of successful experiences," Phys. Rev. Phys. Educ. Res. **13**, 020136 (2017).
[12]For example, OEQuest sells model FML-15-M for 12900 USD.
[13]K. Tamura, E. P. Ippen, H. A. Haus, and L. E. Nelson, "77-fs pulse generation from a stretched-pulse mode-locked all-fiber ring laser," Opt. Lett. **18**, 1080–1082 (1993).
[14]K. Tamura, L. E. Nelson, H. A. Haus, and E. P. Ippen, "Soliton versus nonsoliton operation of fiber ring lasers," Appl. Phys. Lett. **64**, 149–151 (1994).
[15]Tsung-Han Wu, K. Kieu, N. Peyghambarian, and R. J. Jones, "Low noise erbium fiber fs frequency comb based on a tapered-fiber carbon nanotube design," Opt. Express **19**, 5313–5318 (2011).
[16]H. A. Haus, K. Tamura, L. E. Nelson, and E. P. Ippen, "Stretched-pulse additive pulse mode-locking in fiber ring lasers: Theory and experiment," IEEE J. Quantum Electron. **31**(3), 591–598 (1995).
[17]L. E. Nelson, D. J. Jones, K. Tamura, H. A. Haus, and E. P. Ippen, "Ultrashort-pulse fiber ring lasers," Appl. Phys. B **65**, 277–294 (1997).
[18]Govind P. Agrawal, *Nonlinear Fiber Optics* (Academic Press, San Diego, 1995).
[19]Bahaa E. A. Saleh and Malvin C. Teich, *Fundamentals of Photonics*, 2nd ed. (Wiley-Interscience, Hoboken, NJ, 2007).
[20]*Rare Earth Doped Fiber Lasers and Amplifiers*, 2nd ed., edited by Michel J. F. Digonnet (Marcel Dekker Inc., New York, 2001).
[21]Jean-Claude M. Diels, Joel J. Fontaine, Ian C. McMichael, and Francesco Simoni, "Control and measurement of ultrashort pulse shapes (in amplitude and phase) with femtosecond accuracy," Appl. Opt. **24**, 1270–1282 (1985).
[22]Jean-Claude Diels and Wolfgang Rudolph, *Ultrashort Laser Pulse Phenomena* (Academic, New York, 2006).
[23]Andrew M. Weiner, *Ultrafast Optics* (Wiley, New York, 2009).
[24]E. B. Treacy, "Compression of picosecond light pulses," Phys. Lett. A **28**, 34–35 (1968).
[25]R. L. Fork, C. H. Brito Cruz, P. C. Becker, and C. V. Shank, "Compression of optical pulses to six femtoseconds by using cubic phase compensation," Opt. Lett. **12**, 483–485 (1987).
[26]BATOP, for example, sells both semiconductor-based and carbon nanotube based saturable absorbers.
[27]J. W. Nicholson, R. S. Windeler, and D. J. DiGiovanni, "Optically driven deposition of single-walled carbon-nanotube saturable absorbers on optical fiber end-faces," Opt. Express **15**, 9176–9183 (2007).
[28]L. C. Sinclair, J.-D. Deschênes, L. Sonderhouse, W. C. Swann, I. H. Khader, E. Baumann, N. R. Newbury, and I. Coddington, "Invited article: A compact optically coherent fiber frequency comb," Rev. Sci. Instrum. **86**, 081301 (2015).
[29]Yung-Hsiang Lin, Jui-Yung Lo, Wei-Hsuan Tseng, Chih-I. Wu, and Gong-Ru Lin, "Self-amplitude and self-phase modulation of the charcoal mode-locked erbium-doped fiber lasers," Opt. Express **21**, 25184–25196 (2013).
[30]Peter A. Krug, Mark G. Sceats, G. R. Atkins, S. C. Guy, and S. B. Poole, "Intermediate excited-state absorption in erbium-doped fiber strongly pumped at 980 nm," Opt. Lett. **16**, 1976–1978 (1991).
[31]K. W. Su, H. C. Lai, A. Li, Y. F. Chen, and K. F. Huang, "InAs/GaAs quantum-dot saturable absorber for a diode-pumped passively mode-locked Nd:YVO_4 laser at 1342 nm," Opt. Lett. **30**, 1482–1484 (2005).
[32]S. M. J. Kelly, "Characteristic sideband instability of periodically amplified average soliton," Electron. Lett. **28**, 806–807 (1992).
[33]H. A. Haus, C. V. Shank, and E. P. Ippen, "Shape of passively mode-locked laser pulses," Opt. Commun. **15**, 29–31 (1975).

[34]Rick Trebino and Daniel J. Kane, "Using phase retrieval to measure the intensity and phase of ultrashort pulses: Frequency-resolved optical gating," J. Opt. Soc. Am. A **10**, 1101–1111 (1993).
[35]L. P. Barry, P. G. Bollond, J. M. Dudley, J. D. Harvey, and R. Leonhardt, "Autocorrelation of ultrashort pulses at 1.5 μm based on nonlinear response of silicon photodiodes," Electron. Lett. **32**, 1922–1923 (1996).
[36]Jinendra K. Ranka, Alexander L. Gaeta, Andrius Baltuska, Maxim S. Pshenichnikov, and Douwe A. Wiersma, "Autocorrelation measurement of 6-fs pulses based on the two-photon-induced photocurrent in a GaAsP photodiode," Opt. Lett. **22**, 1344–1346 (1997).
[37]S. Y. Set, H. Yaguchi, Y. Tanaka, and M. Jablonski, "Ultrafast fiber pulsed lasers incorporating carbon nanotubes," IEEE J. Sel. Top. Quantum Electron. **10**(1), 137–146 (2004).
[38]Jinkang Lim, Kevin Knabe, Karl A. Tillman, William Neely, Yishan Wang, Rodrigo Amezcua-Correa, François Couny, Philip S. Light, Fetah Benabid, Jonathan C. Knight, Kristan L. Corwin, Jeffrey W. Nicholson, and Brian R. Washburn, "A phase-stabilized carbon nanotube fiber laser frequency comb," Opt. Express **17**, 14115–14120 (2009).
[39]Dylan C. Yost, "Resource letter FCA-1: Frequency combs and applications," Am. J. Phys. **85**, 733–740 (2017).

AJP Index to Advertisers